European Conference on Computational Fluid Dynamics
ECCOMAS CFD 2006
P. Wesseling, E. Oñate and J. Périaux (Eds)

LARGE EDDY SIMULATION OF TWO-PHASE REACTING FLOWS

B. Cuenot*, M. Boileau*, S. Pascaud†, J.-B. Mossa††, E. Riber*, T. Poinsot and C. Bérat†**

*CERFACS
42, Avenue G. Coriolis 31057 Toulouse, France
e-mail: cuenot@cerfacs.fr
web page: http://www.cerfacs.fr
† Turbomeca, (SAFRAN group), Bordes, France
†† Airliquide, Jouy-en-Josas, France
** CERFACS and IMFT - CNRS, Toulouse, France

Key words: Fluid Dynamics, Combustion, Two-phase flows, Large Eddy Simulation, Ignition

Abstract. *Large Eddy Simulation (LES) is now recognized as an efficient numerical tool to predict gaseous combustion in industrial burners, and a number of examples of applications can be found in the literature. In these examples, the accuracy and the predictive capacity of LES are clearly demonstrated, even for unsteady phenomena.*
However most industrial burners are fed with liquid fuel and require the description of droplets dispersion, evaporation and burning. The presence of liquid fuel strongly modifies the fuel vapor distribution in the chamber, leading to different flame ignition and stabilisation processes, as well as different flame structures. Extending the LES technique to two-phase reacting flow is therefore crucial to capture and predict the behavior of such burners.
This has been done in the code AVBP, coupling an eulerian solver for the liquid spray with a LES solver for the gas flow. This approach allows to work on unstructured grids and therefore to calculate the flow in complex geometries. In the present paper, the main steps of the extension of LES to two-phase flow are described and an example of validation is given. Then the solver is applied to the Vesta combustor of Turbomeca, composed of 18 main burners ignited by two pilot flames. This illustrates the capacity of LES to compute complex two-phase reacting flows in transient regimes. To demonstrate LES efficiency, some results will be shown for a calculation done on the IBM supercomputer BlueGene/L - cited by TOP500 as the world's fastest machine - where the use of 2048 parallel processors has enabled to start computing on the full combustor domain (i.e. 18 main injectors + 2 pilot flames).

1 INTRODUCTION

The main part of the production of energy comes from combustion of liquid hydrocarbon fuels, because of their convenient way of storage and transport. Most of the current combustion chambers burn liquid fuel using injectors which atomise, generally at high pressures, the liquid jet or film in small droplets (typically $10 - 200\ \mu m$). Then, the fuel becomes gaseous and an inhomogeneous mixing of air and vaporised fuel is created. For reasons of simplicity, this first step of atomisation is supposed to be instantaneous and numerical tools for evaporation and gaseous combustion are applied to two-phase flow combustors. This allows to study the influence of the liquid phase on steady flames and ignition sequences.

In this paper Large Eddy Simulations (LES) is used to understand unsteady phenomena occurring in turbulent spray combustion. Many proofs of the LES capabilities are available for gaseous combustion (Desjardins[1], Colin[2], Angelberger[3], Pitsch[4], Pierce[5], Selle[6]) but very few studies deal with the complex topic of LES for two-phase reacting flows (Mahesh[7],Mahesh[8],Apte[9],Ham[10]).

The modelling of the liquid phase in a LES solver is an important issue for which two classes of methods are available : the Euler framework (EF) and the Lagrange framework (LF). The LF (Mahesh[7]) describes the liquid phase as a huge but finite number of droplets with their own trajectory, velocity, temperature and diameter while the EF (Pandya[11],Riber[12]) considers the liquid phase as a continuous field whose characteristics are determined through a set of conservation equations for the liquid volume fraction, the liquid phase average velocity and temperature, and the first/second order moments of the size distribution. Several complex phenomena like droplet/droplet coalescence and collision or droplet/wall interaction are easier to model in a LF. However, LES in complex geometries needs high CPU time and requires parallel computing. The efficient implementation of LF on a parallel computer is a critical issue and implies good load balancing (Garcia[13]), whereas EF is directly parallelised with the same algorithms as the gas phase. Moreover, as the LES technique is less dissipative than RANS methods, the number of Lagrangian droplets at each time step in each cell must be sufficient to provide a smooth and accurate continuous field of gaseous fuel. Because the fuel vapour distribution, directly produced by the discrete droplet evaporation source terms, controls the propagation of the front (Pitsch[14], Selle[15]), this is crucial for two-phase flame computations. Very limited experience on this question is available today but it is likely that combustion requires much more particles than usually done for dispersion or evaporation studies, leading to uncontrolled CPU costs.

Finally the atomisation complexity makes the accurate determination of the spray characteristics a critical issue. Even if LF calculates droplet trajectories with precision, very approximate injection conditions will lead to rough results. In gas turbines, airblast injectors are used where the liquid sheet breaks up under the effect of a surrounding swirled flow. Modern Diesel engines injectors use very highly pressurized flows. In both cases

the liquid spray close to the injector is organised as dense blobs (Reitz[16]) and LF can not be applied to these high-loaded zones. As a contrary, EF is more compatible with the physics of liquid injection.
Considering the objectives of the present work, the Euler framework appears to be the best choice in terms of modelling and computing efficiency.

2 COMPUTING METHOD

2.1 Numerical Tool

The solver *AVBP*, developed at *CERFACS*, is a parallel fully compressible code which computes the turbulent reacting two-phase flows, on both structured and unstructured grids, for complex industrial applications such as ignition sequences or acoustic instabilities. It uses explicit finite volume based on a cell-vertex discretisation and a second order time and space Lax-Wendroff centred numerical scheme (Hirsch[17]). As acoustics are explicitely solved for, the time step is controlled by the speed of sound. Characteristic boundary conditions NSCBC (Poinsot[18]) are used. A specificity of AVBP is its ability to run with a very good efficiency on a high number of parallel processors, as will be shown in the last section.

Turbulent combustion modelling is ensured by the Dynamically Thickened Flame model (Legier[19]), using a thickening factor F and an efficiency function E to determine the flame front turbulent velocity (Colin[20]). Subgrid scale turbulent viscosity is defined by the WALE model (Nicoud[21]), derived from the classic Smagorinsky model. The Euler/Euler framework governing a turbulent reacting two-phase flow is composed, for each phase, of a set of conservative equations defined by Eq. (1) and Eq. (2) and solved with the same numerical approach.

$$\text{Carrier phase} \qquad \frac{\partial \overline{\mathbf{w}}}{\partial t} + \nabla \cdot \overline{\mathbf{F}} = \overline{\mathbf{s}} \tag{1}$$

$$\text{Dispersed phase} \qquad \frac{\partial \overline{\mathbf{w}}_l}{\partial t} + \nabla \cdot \overline{\mathbf{F}}_l = \overline{\mathbf{s}}_l \tag{2}$$

For the carrier phase, the vector of conservative variables is defined by Eq. (3) with ρ the density, (u_1, u_2, u_3) the velocity components, $E_t = u_i^2/2 + e_s$ the total non chemical energy (e_s is the sensible energy) and Y_k the fuel mass fractions. The flux tensor $\overline{\mathbf{F}}$ is composed of viscous, inviscid and subgrid scale components and $\overline{\mathbf{s}}$ is the source term defined by Eq. (4). Combustion terms are the reaction rate $\overline{\dot{\omega}}_k$ and the heat release $\overline{\dot{\omega}}_T$ modelled by an Arrhenius law (Poinsot[22]). Additional source terms representing exchanges between phases are the mass transfer $\overline{\Gamma}$, the momentum transfer $\overline{I_i}$ and the enthalpy transfer $\overline{\Pi}$.

$$\overline{\mathbf{w}} = (\overline{\rho}\tilde{u}_1, \overline{\rho}\tilde{u}_2, \overline{\rho}\tilde{u}_3, \overline{\rho}\tilde{E}_t, \overline{\rho}\tilde{Y}_k) \tag{3}$$

$$\overline{\mathbf{s}} = (\overline{I_1}, \overline{I_2}, \overline{I_3}, \frac{E}{F}\overline{\dot{\omega}}_T + \overline{I_i}\tilde{u}_i + \overline{\Pi} + \overline{\dot{\omega}}_{spark}, -\frac{E}{F}\overline{\dot{\omega}}_k + \overline{\Gamma}\delta_{kF}) \tag{4}$$

For the dispersed phase, the vector of conservative variables $\overline{\mathbf{w}}_l$ is defined by Eq. (5) with α_l the volume fraction, $(u_{1,l}, u_{2,l}, u_{3,l})$ the velocity components, $h_{s,l}$ the sensible enthalpy and n_l the droplet number density. The flux tensor $\overline{\mathbf{F}}_l$ is only composed of convective terms and the source term $\overline{\mathbf{s}}$ is defined by Eq. (6).

$$\overline{\mathbf{w}}_l = (\overline{\alpha}_l\overline{\rho}_l, \overline{\alpha}_l\overline{\rho}_l\tilde{u}_{1,l}, \overline{\alpha}_l\overline{\rho}_l\tilde{u}_{2,l}, \overline{\alpha}_l\overline{\rho}_l\tilde{u}_{3,l}, \overline{\alpha}_l\overline{\rho}_l\tilde{h}_{s,l}, \overline{n_l}) \quad (5)$$

$$\overline{\mathbf{s}}_l = (-\overline{\Gamma}, -\overline{I_1}, -\overline{I_2}, -\overline{I_3}, -\overline{\Pi}, 0) \quad (6)$$

This set of equations only describes the statistic average movement of the particles in the cell. The velocity deviation from this average is called the random uncorrelated motion (RUM) and describes the independent movement of each particle. It is an unknown quantity and has to be modeled, as proposed in Kaufmann[23] or Simonin[24] .
In the context of LES, the conservative variables for the dispersed phase are filtered, exactly in the same sense that the gaseous conservative variables. Therefore as for the gaseous phase, a subgrid scale (SGS) model is needed, as proposed for example in Riber[25]. The development of models for the RUM and SGS movement of the droplets is a difficult and complex topic that is still under investigation. It is however established that they are required for an accurate prediction of turbulent droplet dispersion.
A last difficult point in the context of the EF for the dispersed phase is the description of the droplets size distribution. As the drag force and the evaporation rate are directly linked to the droplet diameter, it is crucial to take it into account. This has been recently done in (Mossa[26]), by introducing a presumed-shape size distribution. Then the problem reduces to the computation of higher order moments of the average quantities, for which conservation equations are solved. A delicate point is the unknown size-velocity correlation, required to correctly estimate the drag force. There again a presumed shape is assumed.

3 EXAMPLE OF VALIDATION : THE SOMMERFELD-QIU[27] EXPERIMENT

The configuration of Sommerfeld-Qiu[27] has already been used for the validation of polydisperse models (Apte[28]). The detailed experimental data (mean and fluctuating velocity, droplet size distribution, velocity-droplet size correlation, etc ...) allows a direct comparison with both Lagrangian or Eulerian models. Moreover, the small volume fraction and the low level of droplet interactions with the wall make it compatible with the transport model used here. A parallel primary flow with glass particles is surrounded by an annular swirling secondary flow without particles (Fig. 1). Both flows become highly turbulent after a sudden expansion and the particles are pushed towards the walls by the centrifugal force due to the swirl. The mesh is of 750000 nodes and 4,5 millions cells (see details on Fig.1). The experimental velocity profile is imposed at the inlet. For this case the Stokes number based on the mean diameter is close to 1 and the particles Reynolds number is 12.

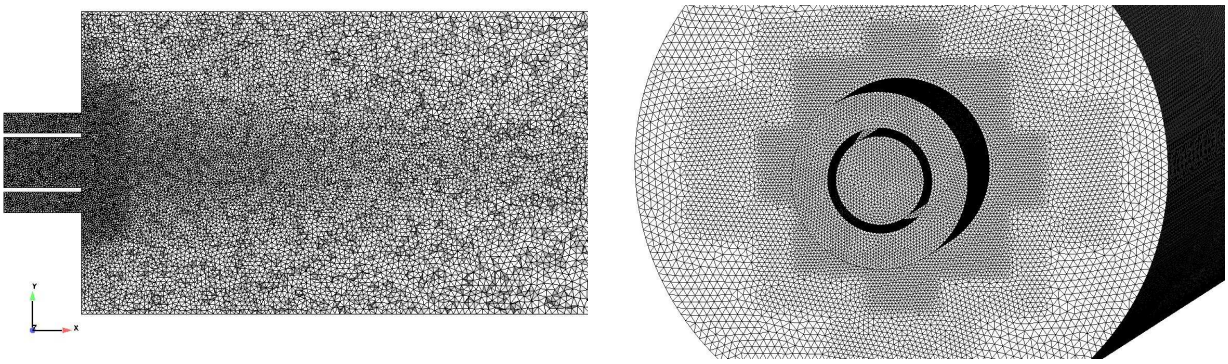

Figure 1: Mesh of the injector

Mean and fluctuating axial velocity profiles at different locations are shown on Figs. 2 and 3 for the gas phase and on Fig. 4 and 5 for the liquid phase. The comparison with the experimental data (incomplete at the first probe position) shows a good agreement for both phases. The radial expansion of the jet is well captured. This is a direct consequence of the high shear stress between the two injected flows, generating high turbulence that expands the initially parallel flow. The velocity profiles for the liquid phase show the entrainment through the drag force of the small particles to the borders of the jet, while the larger droplets follow a straight trajectory around the centerline. This is confirmed by the droplet diameter distribution shown on Fig. 6. The profile in the last measurement plane at $x = 0.155m$ is somewhat different from the experimental data, showing a too fast expansion of the spray, probably due to the error on axial gas velocity visible at locations between $x = 0.085m$ and $x = 0.155m$. This is an example of the impact of the gaseous flow on the droplets through the drag force: a small error in gas velocity may result in a more significant error on the droplets velocity.
Fluctuating velocity profiles have the correct level and overall shape for both phases. Lagrangian simulations (Apte[28]) showed a better agreement with measurements than the simulations reported here (comparison may be found in Mossa[26]), but the grid resolution was much higher, close to Direct Simulation conditions. The present results show then again the capacity of LES and the associated SGS models to capture complex flows.

4 EXAMPLE OF APPLICATION: IGNITION OF THE VESTA BURNER

4.1 Configuration

Figure 7 shows an ensemble view of the Vesta combustor from Turbomeca. It is an annular combustor which can be divided into 18 identical sectors. For each sector, the kerosene spray is provided by an aerodynamic main injector which creates a swirled jet. The starting burners themselves are supposed already ignited and are modelled by hot jets. Figure 8 makes a zoom on two sectors to exhibit the limit of the computing domain as a well as the cutting surface C, later used to show some results. Figure 9 is a sketch in the

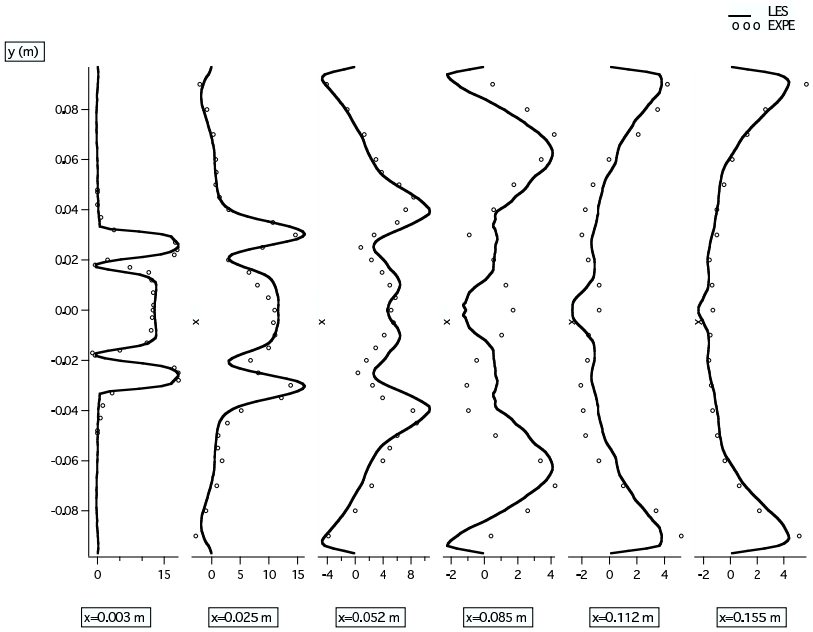

Figure 2: Mean axial velocity of the gas. AVBP_TPF(-), Sommerfeld exp. (○)

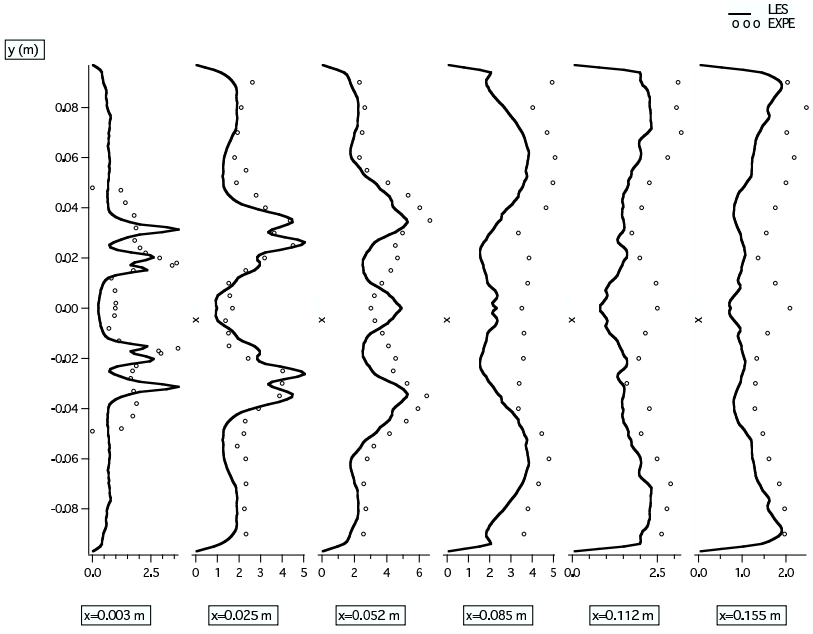

Figure 3: Fluctuating axial velocity of the gas. AVBP_TPF(-), Sommerfeld exp. (○)

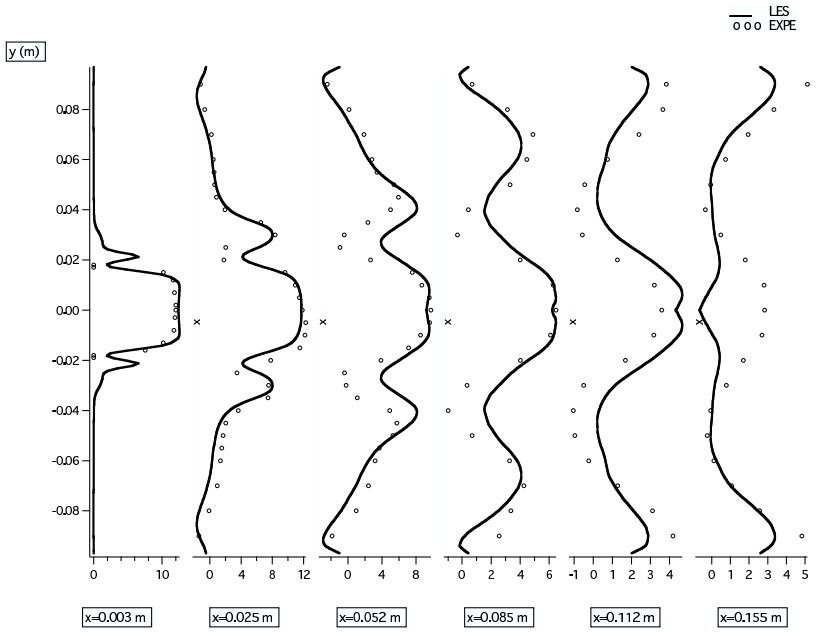

Figure 4: Mean axial velocity of the liquid. AVBP_TPF(-), Sommerfeld exp. (○)

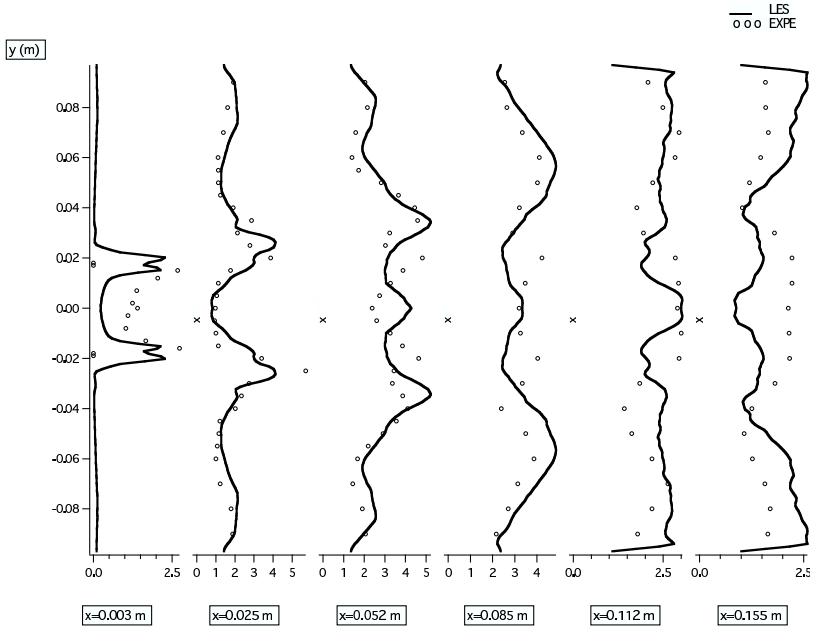

Figure 5: Fluctuating axial velocity of the liquid. AVBP_TPF(-), Sommerfeld exp. (○)

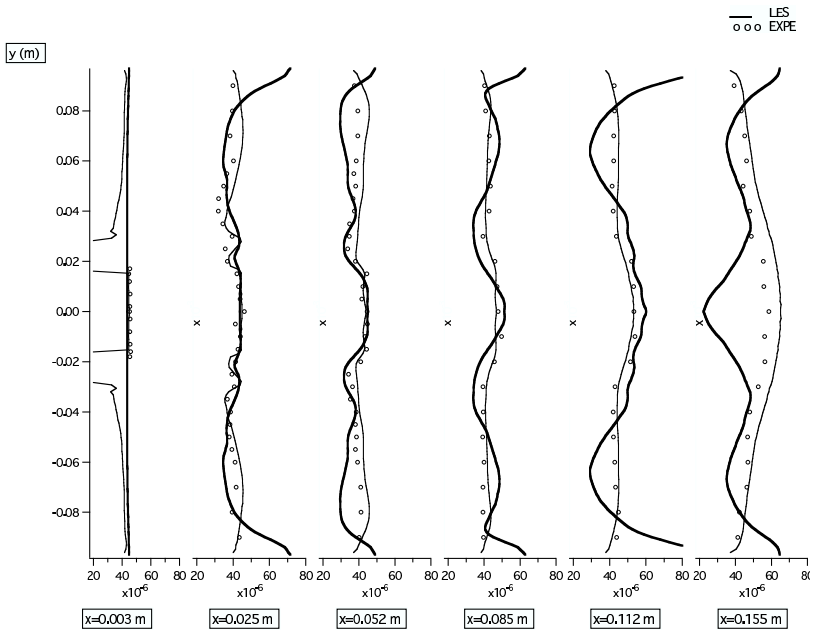

Figure 6: Mean diameter (d_{00}). AVBP_TPF(**-**), Apte and Mahesh[28] (-), Sommerfeld exp ($\circ$)

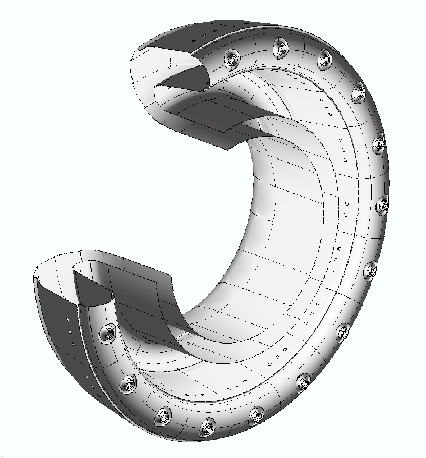

Figure 7: Global view of the Vesta combustor (14 of the 18 sectors are represented).

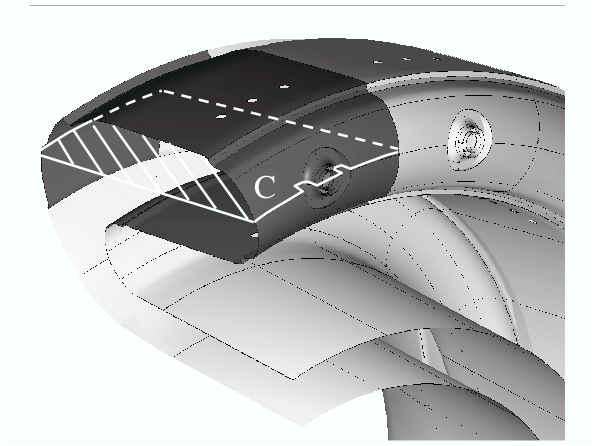

Figure 8: Zoom on two sectors: limit of the computational domain (in dark) and cutting surface C (in white).

C surface that shows how the ignition injector is located between two main injectors. The kerosene injected by such a pressurised injector forms a spray burning with the air coming from the multiple combustor inlets and creating a torch flame. Figure 10 describes how the burning spray has been replaced by a simple jet of hot gas. This gas is the combustion product of a stoichiometric kerosene/air mixture in terms of species composition (CO_2,

H_2O and N_2) and temperature (adiabatic flame temperature). Injecting an inert and hot gas enables to provide some of the burner power, in the form of an enthalpy flux, without adding the complexity of the spark ignition of a fuel spray. In order to stay as realistic as possible, the axis position of the starting injector has been kept and the jet parameters have been calibrated. First, the jet mass flow has been chosen to provide a power corresponding to the combustion of the fuel mass flux. Then, in absence of quantitative experimental data for the real spray, some "good sense" assumptions have been made concerning the jet geometry. So, both diameter and bulk velocity have been calibrated to give a reasonable jet length. It is noticeable that the dynamic effect of this hot jet on the surrounding flow is rather low due the high density ratio between the hot gases and the fresh air. Thus, in order to take into account the spread of the original flame coming from an open spray cone (Fig. 9), a swirling component has been added.
Such simplifications cannot lead to predictable results. Nevertheless, some interesting analysis can be made concerning the processus of ignition and flame propagation in this kind of configuration. A two-phase calculation in a single periodic 20 deg. sector including

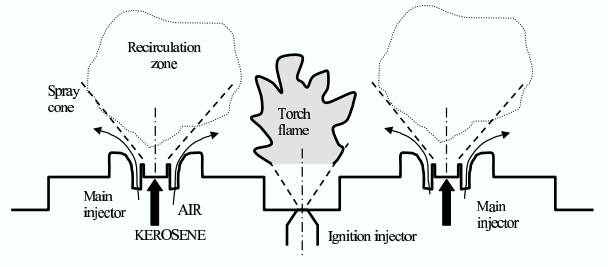

Figure 9: Real configuration

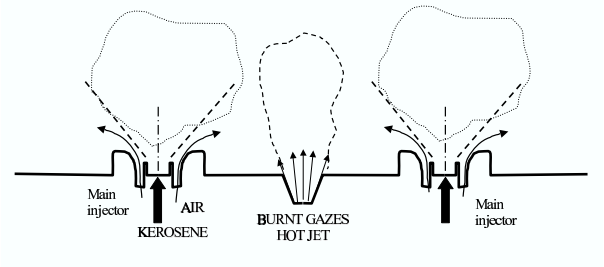

Figure 10: Calculated configuration

one main burner and one hot jet for the starting burner has been computed. Figure 11 describes the boundary surfaces of the computing domain.

The parameters for the boundary conditions are listed in Table 1. The lateral surfaces are set as axi-periodic conditions to be as less restrictive as possible. All the inlets and the outlet are NSCBC (Poinsot[18]) boundaries which are non reflecting for acoustic waves. The computing domain does not include the full swirler geometry of the main injector. So, the imposed velocity profile has been calibrated using a previous non reactive LES calculation in an extended domain taking into account the complexity of the whole swirler geometry. The real combustor also has cooling films and multi-perforated walls which are not included here because they would add useless complexity in relation to the objectives of this work. Finally, one can notice that the physical boundary parameters are not favourable for ignition in terms of air and fuel jets temperature and droplets size. However, these values correspond to real starting conditions for a typical helicopter gas turbine. The entire domain has been meshed using tetrahedral cells with a good refinement around the inlets and in the combustion zone (Fig. 12). The obtained grid has 1.03 million cells and

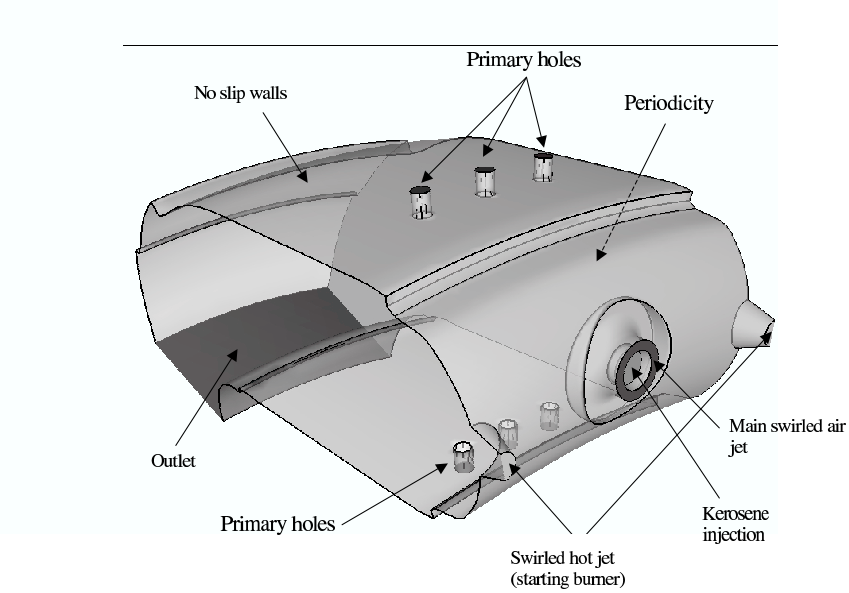

Figure 11: Computing domain of the single sector calculation

178 thousand nodes.

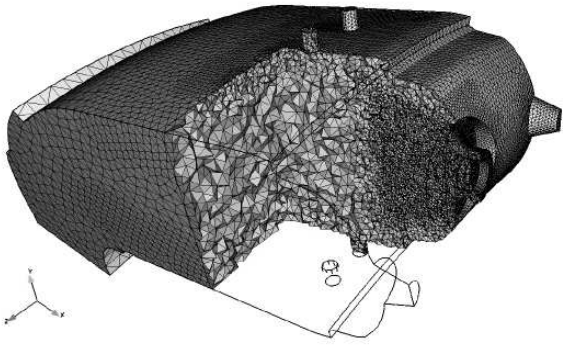

Figure 12: View of the computing tetrahedral grid

In order to be as close as possible to the real ignition conditions, the initial condition of the run is the one of a steady non reactive flow where liquid kerosene is injected but weakly prevaporized. At the beginning of the calculation, the hot jet flux is applied with a relaxation time avoiding introduction of excessive acoustic perturbation.
A 52.6 ms ignition sequence was calculated on a SGI Origin 3800 using 64 parallel processors and took around 100 hours of execution time.

Name	**Boundary type**	**Physical parameters**
Primary holes	inlet (jet in cross flow)	Air at $T = 273\ K$
Main injector	Inlet (2 swirled contrarotating jets)	Air at $T = 273\ K$, Monodisperse spray of kerosene droplets: size $d = 100\ \mu m$ $T = 273\ K$
Hot jet	Inlet (swirled jet)	Burnt gas mixture at $T = 2400\ K$
Combustor walls	Wall	No slip, Adiabatic
Outlet	Pressure imposed	$p = 1.18\ bar$

Table 1: Boundary conditions

4.2 Results

Figure 13 illustrates the temporal variation of relevant quantities through the ignition sequence. During the first ten milliseconds, the hot jet increases the gas mean temperature. The fuel droplets carried in the hot environment of the jet evaporate faster producing fuel vapor and inducing two phenomena:

1. A reaction zone takes place around the hot jet where the high temperature enables to maintain a sufficient evaporation rate. During the first 15 ms, this reaction only consumes a low part of the liquid fuel as shown by the reaction and evaporation rates plots (Fig. 13, right graph).

2. The unburnt fuel is blown downstream and its vaporisation creates an accumulation of gaseous fuel downstream the primary zone. Once mixed with air and heated by the hot jets, this fuel vapor burns fast releasing a great amount of heat (Fig. 13, left graph).

3. This heat release induces a strong pressure wave which disturbs the inlet fluxes as shown by the hot jet curve on the left graph of Fig. 13. At this time, the reactive zone coming from the hot jet is entering the central recirculating zone created by the vortex breakdown of the main injector inlet.

4. Once the recirculating zone is filled by hot gases, the flame is stabilising in front of the swirled jet. Even after the hot jet has been cut off (at 38.7 ms), the combustion stays stable with an equilibrium between the evaporation rate and the burning rate (Fig. 13, right graph) as well as an almost steady mean gas temperature (Fig. 13, left graph).

To better understand what happens in the primary zone, Fig. 14 exhibits some key variables of the flow on the cutting surface C (Fig. 8) for different times of the ignition process. Although this two-dimension view stays restrictive for a three-dimension flow, it is still

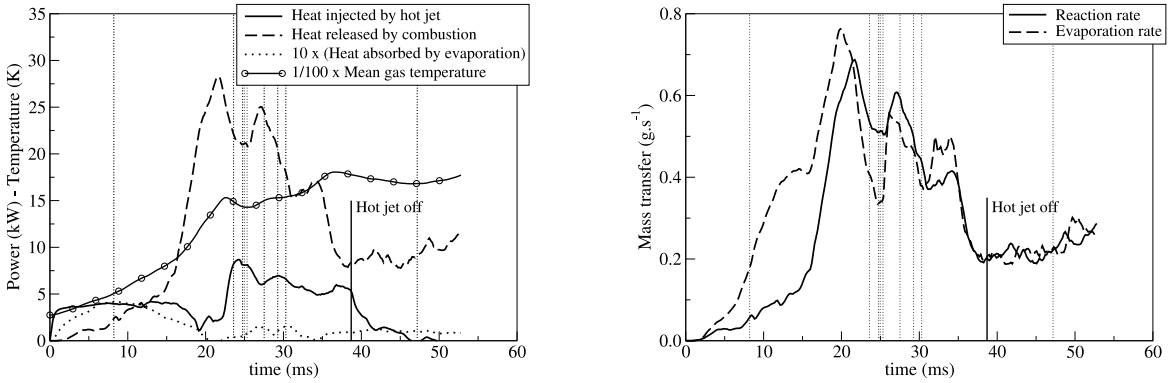

Figure 13: Temporal evolution of various total quantities in the domain. Left: energy transfers and gas temperature. Right: mass transfers. The vertical lines indicate the instants of the 9 snapshots featured in Fig. 14.

relevant to see how combustion propagates from the ignitor region to the main injection zone.

First, the 8.21 ms snapshot illustrates how the main swirl jet induces a vortex breakdown with an intense recirculating zone. This phenomenon has been described by Lucca-Negro[29] and is known to be a stabilising mechanism for jet combustion. This snapshot also shows that the recirculating zone stays poorly influenced by the surrounding hot jet as the reactive zone is kept outside the back flow line. Nevertheless, some hot gases are sporadically captured leading to an increasing mean temperature inside the back flow line, as shown on the 23.59 ms snapshot. At 24.75 ms, a part of the hot jet flame is entering the back flow zone and seems to be extinguished before propagating up to the main injection (time 24.96 ms and 25.33 ms). Thanks to the heat released by the passage of this flame, gaseous fuel becomes more present in the region close to the vortex breakdown. This enables a strong flame to propagate to that place at around 27.52 ms. However, until the whole recirculating zone is not fulled by hot gases, this flame is not stable yet (29.26 ms snapshot). Finally, from 30.30 ms, where a high temperature can be found almost everywhere in the primary zone, until the end of the simulation, a stable combustion is observed in the main burner.

The 47.18 ms illustrates the steady configuration of the reactive flow, featuring:

- A primary reactive zone (solid line) anchored to the main injector. It corresponds to a diffusion flame fed by the air coming from the external swirler of the main injector and the vaporisation of the liquid kerosene spray injected by the internal swirler.
- A secondary and downstream flame (dashed line) burning the excess of fuel with the air injected by the transversal primary holes.
- The tracks of a row of these primary jets appears through three cold spots (dotted

lines) that one can distinguish in the temperature field.

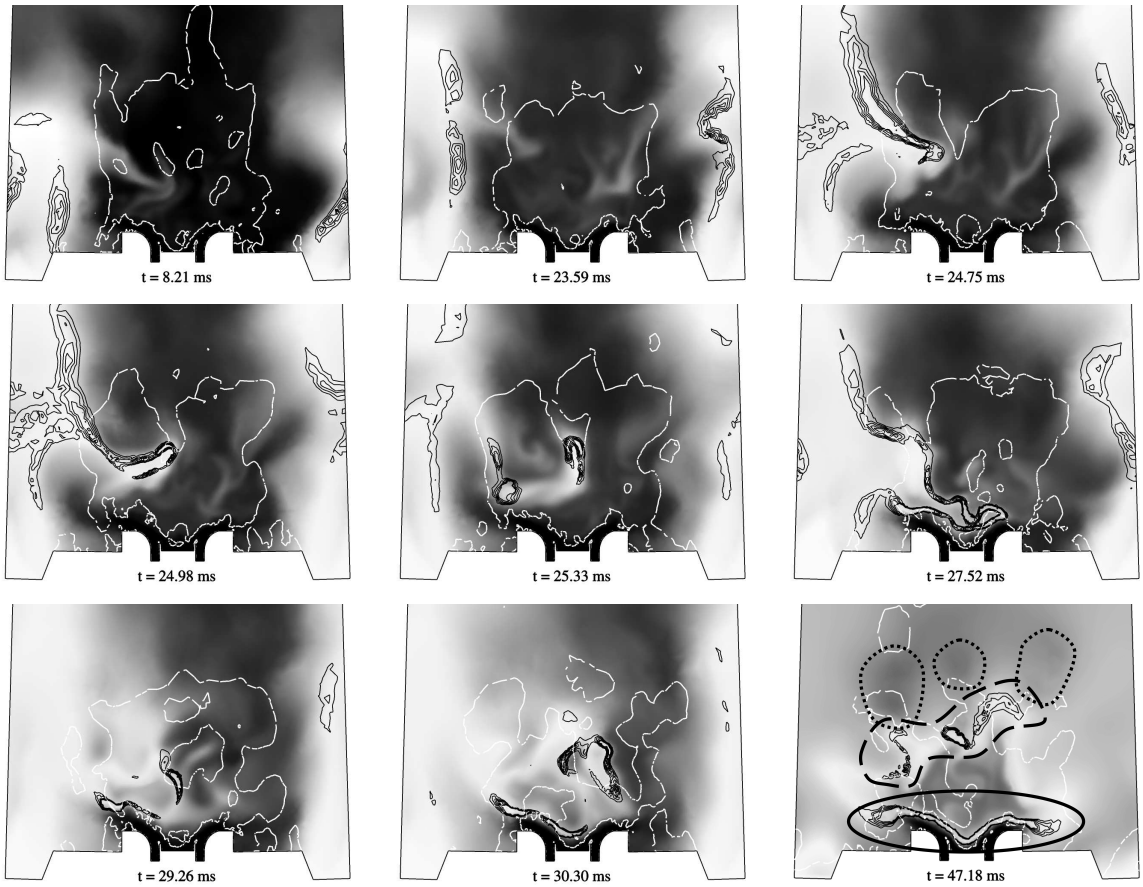

Figure 14: Propagation of the reactive zone from the hot jet to the main injector on cutting surface C. Grey scale: gas temperature (black: 273 K → white: 2400 K). Black lines: reaction rate isolines. White lines: isolines of 0 axial velocity (back flow lines).

5 SIMULATION OF IGNITION IN THE FULL BURNER

Direct visualisation and results from multi-burners simulations show that ignition is a process involving the full burner geometry. Therefore a simulation has been performed on the complete annular Vesta burner. The parameters for this calculation are the same as in the previous section with the following differences:

1. Due to technical and timing constraints, the liquid kerosene spray has been replaced by an equivalent injection of gaseous kerosene. This new injection has the same mass flux and the same profiles for concentration and velocity than the previous liquid one.

2. Periodicity condition is removed since 360 deg. are computed.

3. Among the 18 sectors, two hot jets are used to represent the two real starting burners (Fig. 15).

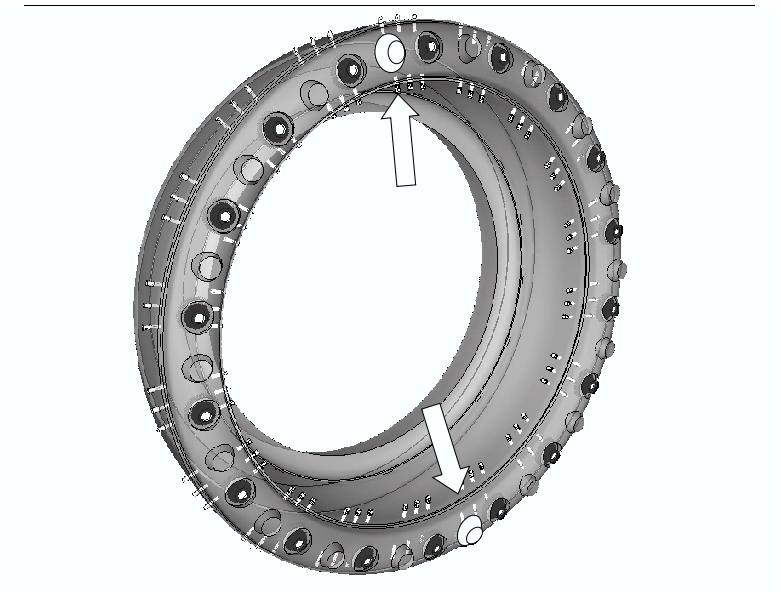

Figure 15: Computing domain and boundary conditions of the full combustor. White arrows point the hot jets location.

The 360 deg. grid has been produced by replicating periodically the original 20 deg. grid. This final grid is composed of 3.14 million nodes and 18.6 million tetrahedral cells. To handle such a large calculation, the present fastest supercomputer BlueGene/L has been used. BlueGene is an IBM parallel computer equipped with a powerful network which enables efficient runs on thousands of processors. The simulation has been run on a rack of 2048 processors for 10 ms of physical time which corresponds to the beginning of the ignition sequence. Then the run has been continued on 128 processors of the SGI-O3800 at CINES, for a total CPU time of 80,000 hours, allowing to complete the ignition of the full burner. Figure 16 provides a view of the ignition in the full combustor geometry. Although detailed validation by comparison with experiment is not possible (detailed measurements are not available), general trends are qualitatively recovered, like the mechanism of flame propagation from one burner to the other or the time needed to ignite the full burner.

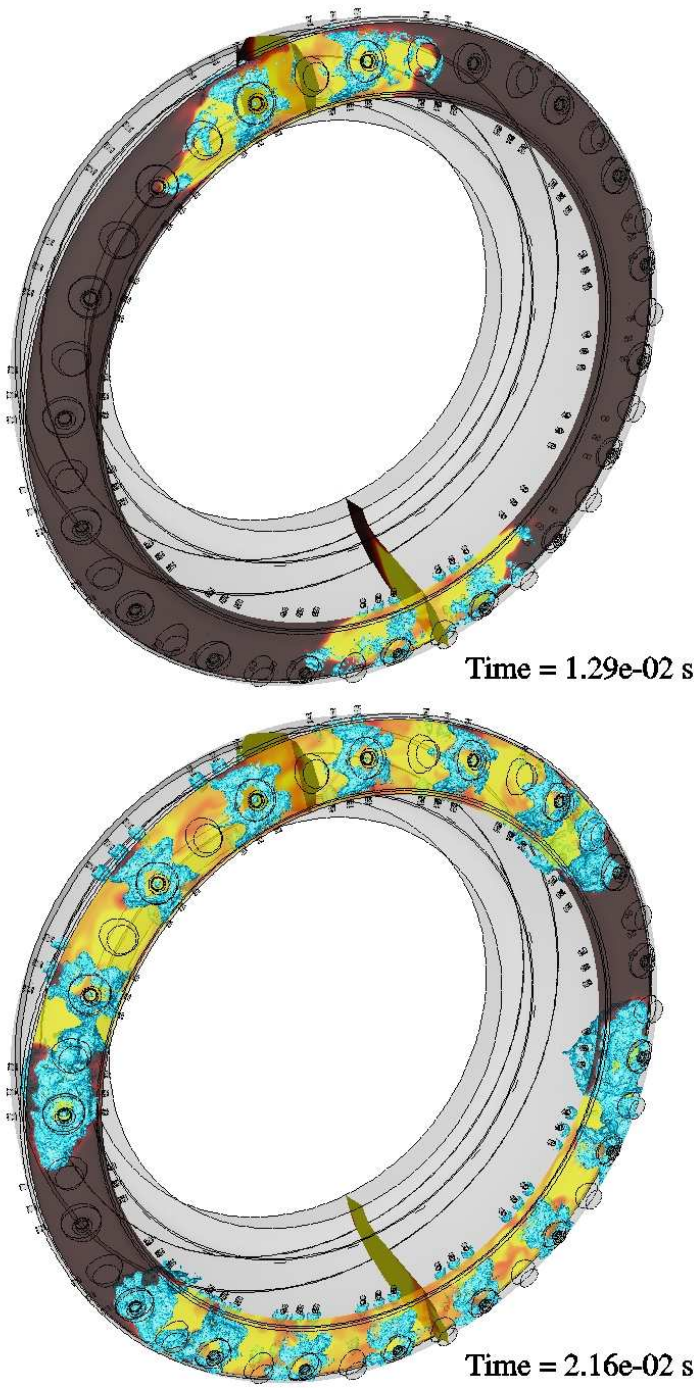

Figure 16: Ignition of the full Vesta combustor. Color scale on clipping surface: gas temperature. Blue surfaces: flame.

6 CONCLUSIONS

The extension of LES to two-phase reacting flows, including polydisperse effects, has been demonstrated on different configurations. A validation test case shows that the mean

features of the liquid phase are well captured, as well as the fluctuation levels and the effect of the droplets size distribution. The simulation of an ignition sequence of an industrial burner illustrates the high potential of LES for transient flow in complex geometries. This relies on a maximum computing efficiency, and a final example is given to show today's computers capabilities for the simulation of large configurations using parallel processing: the complete ignition sequence of a full annular helicopter burner simulation, run on the IBM supercomputer BlueGene/L machine, shows the excellent performance of both the code and the computer and gives to LES a promising perspective for the future.

Acknowledgements
CINES and IBM are gratefuly acknowledged for the computing support.

REFERENCES

[1] P.E. Desjardins and S.H. Frankel. Two dimensional large eddy simulation of soot formation in the near field of a strongly radiating nonpremixed acetylene-air jet flame. *Comb. and Flame*, **119**(1/2), 121–133, (1999).

[2] O. Colin. *Simulation aux Grandes Echelles de la Combustion Turbulente Prémélangée dans les Statoréacteurs*. PhD thesis, INP Toulouse, (2000).

[3] C. Angelberger, F. Egolfopoulos, and D. Veynante. Large eddy simulations of chemical and acoustic effects on combustion instabilities. *Flow Turb. and Combustion*, **65**(2), 205–22, (2000).

[4] H. Pitsch and L. Duchamp de la Geneste. Large eddy simulation of premixed turbulent combustion using a level-set approach. *Proceedings of the Combustion Institute*, **29**, in press, (2002).

[5] C.D. Pierce and P. Moin. Progress-variable approach for large eddy simulation of non-premixed turbulent combustion. *J. of Fluid Mech.*, **504**, 73–97, (2004).

[6] L. Selle. *Simulation aux grandes échelles des couplages acoustique / combustion dans les turbines á gaz*. Phd thesis, INP Toulouse, (2004).

[7] K. Mahesh, G. Constantinescu, S. Apte, G. Iaccarino, F. Ham, and P. Moin. Progress towards large-eddy simulation of turbulent reacting and non-reacting flows in complex geometries. In *Annual Research Briefs*, Center for Turbulence Research, NASA Ames/Stanford Univ., 115–142, (2002).

[8] K. Mahesh, G. Constantinescu, and P. Moin. A numerical method for large-eddy simulation in complex geometries. *J. of Comp. Physics*, **197**, 215–240, (2004).

[9] S. V. Apte, M. Gorokhovski, and P. Moin. Large-eddy simulation of atomizing spray with stochastic modeling of secondary breakup. In *ASME Turbo Expo 2003 - Power for Land, Sea and Air*, Atlanta, Georgia, USA, (2003).

[10] F. Ham, S. V. Apte, G. Iaccarino, X. Wu, M. Herrmann, G. Constantinescu, K. Mahesh, and P. Moin. Unstructured les of reacting multiphase flows in realistic gas turbine combustors. In *Annual Research Briefs - Center for Turbulence Research*, (2003).

[11] R.V.R. Pandya and F. Mashayek. Two-fluid large-eddy simulation approach for particle-laden turbulent flows. *Int. J. of Heat and Mass Transfer*, **45**, 4753–4759, (2002).

[12] E. Riber, M. Moreau, O. Simonin, and B. Cuenot. Towards large eddy simulation of non-homogeneous particle laden turbulent gas flows using euler-euler approach. In *11th Workshop on Two-Phase Flow Predictions*, Merseburg, Germany, 2005.

[13] M. García, Y. Sommerer, T. Schönfeld, and T. Poinsot. Evaluation of euler/euler and euler/lagrange strategies for large eddy simulations of turbulent reacting flows. In *ECCOMAS Thematic Conference on Computational Combustion*, (2005).

[14] H. Pitsch and N. Peters. A consistent flamelet formulation for non-premixed combustion considering differential diffusion effects. *Comb. and Flame*, **114**, 26–40, (1998).

[15] L. Selle, G. Lartigue, T. Poinsot, P. Kaufman, W. Krebs, and D. Veynante. Large eddy simulation of turbulent combustion for gas turbines with r educed chemistry. In *Proceedings of the Summer Program - Center for Turbulence Research*, 333–344, (2002).

[16] R.D. Reitz and R. Diwakar. *Structure of high pressure fuel sprays*. Technical Report Tech. Rep. 870598, SAE Technical Paper, (1987).

[17] C. Hirsch. *Numerical Computation of Internal and External Flows*. John Wiley & Sons, (1989).

[18] T. Poinsot and S. Lele. Boundary conditions for direct simulations of compressible viscous flows. *J. of Comp. Physics*, **101**(1):104–129, (1992).

[19] J.-Ph. Légier, T. Poinsot, and D. Veynante. Dynamically thickened flame large eddy simulation model for premixed and non-premixed turbulent combustion. In *Summer Program 2000*, Center for Turbulence Research, Stanford, USA, 157–168, (2000).

[20] O. Colin, F. Ducros, D. Veynante, and T. Poinsot. A thickened flame model for large eddy simulations of turbulent premixed combustion. *Physics of Fluids*, **12**(7), 1843–1863, (2000).

[21] F. Nicoud and F. Ducros. Subgrid-scale stress modelling based on the square of the velocity gradient. *Flow Turb. and Combustion*, **62**(3), 183–200, (1999).

[22] T. Poinsot and D. Veynante. *Theoretical and numerical combustion, second edition*. R.T. Edwards, (2005).

[23] A. Kaufmann, O. Simonin and T. Poinsot. Direct numerical Simulation of Particle-Laden Homogeneous Isotropic Turbulent Flows Using a Two-Fluid Model Formulation, 5^{th} *Int. Conf. on Multiphase Flow*, ICMF'04, (2004).

[24] O. Simonin, P. Février and J. Laviéville". On the Spatial Distribution of Heavy Particle Velocities in Turbulent Flow: from Continous Field to particulate Choas. *Journal of Turbulence*, **3**, (2002).

[25] E. Riber, M. Moreau, O. Simonin and B. Cuenot. Development of Euler-Euler LES Approach for Gas-Particle Turbulent Jet Flow, *ASME Fluids Engineering Summer Conference*, ASME FED, (2006),

[26] J.-B. Mossa. *Extension Polydisperse pour la Description Euler-Euler des Ecoulements Diphasiques Ractifs* Phd thesis, INP Toulouse, (2005).

[27] Sommerfeld, M. and Qiu, H. Detailed measurements in a swirling particulate two-phase flow by a phase-Doppler anemometer. *Int. Journal Heat and Fluid Flow*, **12**, 20–28, (1991).

[28] Apte, S. V., Mahesh, K., Moin, P., Oefelein, J.-C. Large-eddy simulation of swirling particle-laden flows in a coaxial-jet combustor. *Int. Journal of Multiphase Flow*, **29**, 1311–1331, (2003).

[29] O. Lucca-Negro and T. O'Doherty. Vortex breakdown: a review. *Prog. Energy Comb. Sci.*, **27**:431–481, 2001.